RSC Advances

This article can be cited before page numbers have been issued, to do this please use: F. Xue, W. chen, X. song, X. cheng and Y. Ding, *RSC Adv.*, 2016, DOI: 10.1039/C5RA28075C.

ROYAL SOCIETY OF CHEMISTRY

www.rsc.org/advances

View Article Online
DOI: 10.1039/C5RA28075C

Journal Name

ARTICLE

Promotional effects of Cr and Fe on Rh/SiO_2 catalyst for the preparation of ethanol from CO hydrogenation

Received 00th January 20xx,
Accepted 00th January 20xx

DOI: 10.1039/x0xx00000x

www.rsc.org/

Fei Xue[a, c], Weimiao Chen[a], Xiangen Song[a], Xianbo Cheng[a], Yunjie Ding[a, b]*

A series of Cr and Fe promoted Rh-based silica supported catalysts were prepared by an incipient co-impregnation method. The performance of the catalysts was investigated by the hydrogenation of carbon monoxide to ethanol. The catalysts were characterized by N_2 adsorption-desorption, X-ray diffraction, transmission electron microscopy, H_2 temperature-programmed reduction, temperature programmed surface reaction, and fourier transform infrared spectroscopy. The results revealed that addition of 0.2–0.4 wt% Cr to Rh/SiO_2 increased its activity significantly. However, further addition of 0.1–0.2 wt% Fe lowered CO conversion slightly, while the selectivity towards ethanol was enhanced significantly. Therefore, high catalytic activity and selectivity toward ethanol were achieved by simultaneous introduction of 0.4 wt% Cr and 0.2 wt% Fe to Rh/SiO_2. This may be due to improved dispersion of Rh particles, moderate ability to dissociate CO molecules, and high ratio of Rh^+ sites to Rh^0 sites.

1. Introduction

Ethanol, as a clean fuel, offers the same chemical energy as that of gasoline with less emission of greenhouse gases and other environmental pollutants attracting increasing attention. Currently, ethanol is produced by fermentation of sugars and hydration of petroleum-based ethylene.[1] However, the poor energy efficiency of the fermentation process and depletion of crude oil resources globally have limited the use of ethanol in automobiles. Therefore, development of alternate technologies to synthesize ethanol from syngas (CO and H_2) derived from coal, natural gas, or biomass has attracted global attention in recent years. So far, four types of catalysts have been primarily employed for this conversion: (a) Rh-based catalysts[2–8], (b) modified methanol synthesis catalysts[9,10], (c) modified Fischer–Tropsch catalysts based on Co[11–13], Fe[14], and Ru[15], and (d) modified Mo-based catalysts[16]. Among these catalysts, Rh-based catalysts have been demonstrated to be the most selective catalysts for the synthesis of C_{2+} oxygenates due to the unique CO adsorption behavior on Rh particles. In other words, Rh species are able to simultaneously adsorb CO in both molecular and dissociated states.[17–24]

Extensive studies have shown that promoters are essential for Rh-based catalysts to synthesize C_{2+} oxygenates from syngas and many promoters such as Mn[25], V[26], La[6], and Zr[27] have been used with Rh-based catalysts. Cr_2O_3 has been used as a catalyst[28,29] for alkane dehydrogenation or a structural promoter[30–32] for methanol synthesis from syngas. On the other hand, some studies[1,33] have suggested that the ethanol yield was improved as Rh-based catalysts were supported over Cr_2O_3. However, detailed studies on the role of Cr_2O_3 in the Rh-based catalysts for CO hydrogenation have not yet been addressed. Moreover, the promotion effect of Fe on Rh-based catalysts has been extensively studied.[34–36] Many studies[37,38] have demonstrated that the addition of Fe to Rh-based catalysts can boost the hydrogenation of acetaldehyde to form ethanol and decrease methane selectivity. Therefore, we speculated that the selectivity of the catalyst towards ethanol formation might be increased by combining the merits of both Cr and Fe.

In this study, we investigated the promoting effects of Cr and Fe on silica supported Rh-based catalysts for the synthesis of ethanol from CO hydrogenation.

2. Experimental

2.1 Catalyst preparation

First, SiO_2 (20–40 mesh) was calcined at 800 °C for 6 h prior to its use. Then, the catalysts were prepared by impregnating SiO_2 with an aqueous solution of $RhCl_3 \cdot 3H_2O$, $Cr(NO_3)_3 \cdot 9H_2O$ and $Fe(NO_3)_3 \cdot 9H_2O$. Following impregnation, the catalysts were first dried at room temperature, then dried at 100 °C for 12 h, and finally calcined at 300 °C for 3 h. The amount of Rh in all catalysts was 1.5 wt%. The as-prepared catalysts are labeled as RCF(x, y)/SiO_2, where x, y indicates the contents of Cr and Fe

[a] Dalian National Laboratory for Clean Energy, Dalian Institute of Chemical Physics, Chinese Academy of Sciences, Dalian 116023, PR China
[b] State Key Laboratory of Catalysis, Dalian Institute of Chemical Physics, Chinese Academy of Sciences, Dalian 116023, PR China. Tel.: +86 411 84379143; fax: +86 411 84379143; Email: dyj@dicp.ac.cn (Y. Ding)
[c] University of Chinese Academy of Sciences, Beijing 100049, PR China

View Article Online
DOI: 10.1039/C5RA28075C

respectively (x = 0.0, 0.2, 0.4 or 0.6 wt%; y = 0.0, 0.1, 0.2, or 0.4 wt%, based on SiO_2).

2.2 Catalyst characterization

The specific surface area, pore diameter, and pore volume of the samples were obtained by N_2 adsorption-desorption at −196 °C using a physical adsorption instrument (Quantachrome, USA). Prior to analysis, each sample was pre-treated under vacuum at 120 °C for 3 h.

X-ray diffraction (XRD) patterns were recorded on a PANalytical X' Pert-Pro diffractometer operated at 40 kV and 40 mA using Ni-filtered Cu Kα (λ = 0.15406 nm) radiation.

Transmission electron microscopy (TEM) images were recorded on a JEOL JEM-2100 electron microscope operated at 200 kV.

H_2 temperature-programmed reduction (TPR) was carried out on Altamira Instruments AMI-300 U. First, approximately 100 mg of the catalyst sample was pretreated at 120 °C for 1 h under Ar (99.999% purity) and then cooled to 50 °C. Subsequently, 10% H_2/Ar was introduced with a flow rate of 30 ml/min and the reduction was carried out at a temperature ramp rate of 10 °C/min.

Temperature programmed surface reaction (TPSR) analysis was also performed on Altamira Instruments AMI-300 U. Approximately 100 mg of the catalyst sample was used for each test. Each sample was reduced in situ by 10% H_2/Ar at 350 °C for 2 h, purged with Ar (99.999% purity) at the same temperature for 0.5 h, and then cooled to 50 °C. Then, 10% CO/He was introduced for adsorption for 0.5 h. Subsequently, the sample was flushed with 10% H_2/Ar, while the temperature was increased to 800 °C at the rate of 10 °C /min. The signal of CH_4 (m/z = 16) was recorded by a quadruple mass spectrometer simultaneously.

Fourier transform infrared (FTIR) spectra were collected with a Nicolet iS50 spectrometer. Before each experiment, the samples were pressed into self-supported wafers (ca. 20 mg/cm^2) and reduced in situ in the IR cell under H_2 gas flow (99.999% purity) at 350°C for 2 h. Subsequently, the sample was swept with N_2 (99.999% purity) at 350 °C for 0.5 h, and then cooled to 50 °C. After cooling to 50 °C in N_2, a background spectrum was recorded with spectral resolution of 4 cm^{-1} and scan times of 32. Then the sample was purged with CO (99.999% purity) for 0.5 h, followed by flushing with N_2.

2.3 Activity tests

CO hydrogenation was performed in a fixed-bed micro-reactor (length of 300 mm and internal diameter of 9 mm) at 280 °C, 5.0 MPa (H_2/CO = 2), and gas hourly space velocity (GHSV) = 5000 h^{-1}. The catalyst (0.95 g) and quartz sand (3.0 g) were mixed together to avoid channeling and hot spots, and axially centered in the reactor tube with the temperature monitored by a thermocouple. The catalysts were first reduced in situ in a pure H_2 atmosphere at 350 °C for 2 h, and then the catalyst bed was cooled down to the reaction temperature, followed by the introduction of syngas. The effluent from the fixed-bed reactor was passed through a condenser and subsequently analyzed on-line by an Agilent 3000A Micro GC with a thermal conductivity detector. After the reaction reached stability, the liquid products dissolved in deionized water in the condenser were collected for 5 h and analyzed off-line by an Agilent 7890 GC with a flame ionization detector using n-pentanol as an internal standard. The CO conversion and product selectivity were calculated according to the following equations:

$$\text{CO conversion [\%]} = \frac{\sum n_i \times M_i}{M_{CO}} \times 100 ,$$

$$\text{Selectivity [\%]} = \frac{n_i \times M_i}{\sum n_i \times M_i} \times 100$$

Where n_i was the number of carbon atoms in product i, M_i is the percentage of product i detected, and M_{CO} is the percentage of CO in the syngas feed. The experimental error is about ±5%.

3. Results and discussion

3.1 Catalytic performance

Table 1 lists the results of the CO hydrogenation reaction over Rh-Cr-Fe/SiO_2 catalysts with different loading amounts of Cr and Fe. The CO conversion over Rh/SiO_2 was only 4.6%, and the main product was CH_4. As Cr was added to the Rh/SiO_2, the CO conversion and ethanol selectivity increased significantly, reaching 14.5% and 11.7%, respectively when Cr loading increased to 0.4 wt%. Further increase in the Cr loading amount lowered the catalytic performance. Therefore, the Cr loading was fixed at the optimal 0.4 wt% in the Rh/SiO_2 catalysts when we intended to add the second promoter Fe. It was found that CO conversion decreased slowly. On the other hand, the selectivity towards ethanol reached a maximum of 26.0% as 0.2 wt% Fe was added to Cr-promoted Rh/SiO_2. Further increase in Fe loading caused an abrupt decrease in the CO conversion to 6.1% and the selectivity towards ethanol to 16.1%. In addition, the referenced Fe-promoted Rh/SiO_2 with Fe loading of 0.2 wt% was also prepared and investigated in CO hydrogenation. It was found that the CO conversion changed little compared with Rh/SiO_2; and that the selectivity towards ethanol was only 14.8%.

3.2 N_2 adsorption results

The N_2 adsorption results of the support and catalysts are shown in Table 2. The specific surface area, pore size, and total pore volume for the support and catalysts were in the range of 133.0–138.0 m^2/g, 8.60–8.75 nm, and 0.78–0.85 cm^3/g, respectively. The composition of catalysts had little effect on the physical properties of the catalysts, which might be due to the low metal loading. Therefore, the physical properties of the catalysts are likely not the major factor influencing the catalytic performance.

View Article Online
DOI: 10.1039/C5RA28075C

Table 1 Results of CO hydrogenation over Rh-based catalysts with loading amounts of promoters [a]

Cr (wt%)	Fe (wt%)	CO conversion (%)	Selectivity of products (C %)							
			CH_4	C_{2+} HC [b]	CO_2	MeOH [c]	HAc [d]	EtOH [e]	HOAc [f]	C_{2+}Oxy [g]
0.0	0.0	4.6	71.3	14.7	0.2	0.0	8.8	3.0	0.0	2.0
0.2	0.0	10.5	69.1	12.0	0.0	0.5	8.6	7.9	0.1	1.8
0.4	0.0	14.5	64.6	11.1	0.0	0.8	8.3	11.7	1.2	2.3
0.6	0.0	9.1	72.1	9.1	0.0	0.6	5.5	10.3	0.6	1.8
0.0	0.2	5.4	43.4	0.8	0.8	39.6	0.0	14.8	0.0	0.6
0.4	0.1	14.0	66.8	5.6	0.0	3.0	2.6	19.7	0.7	1.6
0.4	0.2	10.2	58.2	2.5	0.0	10.5	0.9	26.0	0.0	1.9
0.4	0.4	6.1	62.0	1.2	0.5	19.2	0.0	16.1	0.0	1.0

[a] Reaction conditions: 0.95 g catalyst, 3.0 g quartz sand, 280 °C, 5 MPa, $H_2/CO = 2$, GHSV = 5000 h^{-1}. [b] Hydrocarbons with more than two carbon atoms. [c] Methanol. [d] Acetaldehyde. [e] Ethanol. [f] Acetic acid. [g] Oxygenates with more than two carbon atoms.

Table 2 Physical properties of the support and catalysts

Catalysts	Specific surface area (m^2/g)	Pore size (nm)	Pore volume (cm^3/g)
SiO_2	137.5	8.69	0.84
RCF(0.0, 0.0)/SiO_2	134.4	8.73	0.80
RCF(0.0, 0.2)/SiO_2	133.6	8.69	0.80
RCF(0.4, 0.0)/SiO_2	134.9	8.71	0.78
RCF(0.4, 0.2)/SiO_2	135.9	8.66	0.80

3.3 XRD and TEM analysis

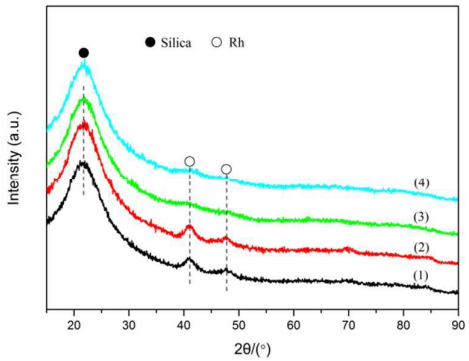

Fig. 1 XRD patterns of reduced RCF(x, y)/SiO_2 catalysts: (1) x = 0.0, y = 0.0; (2) x = 0.0, y = 0.2; (3) x = 0.4, y = 0; and (4) x = 0.4, y = 0.2.

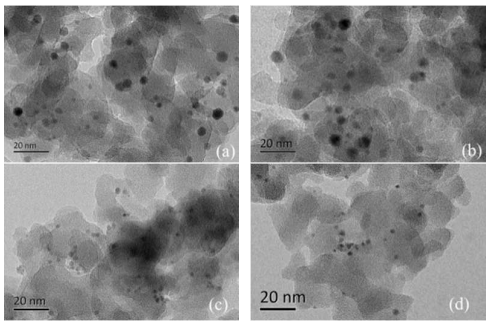

Fig. 2 TEM images of reduced RCF(x, y)/SiO_2 catalysts: (a) x = 0.0, y = 0.0; (b) x = 0.0, y = 0.2; (c) x = 0.4, y = 0.0; and (d) x = 0.4, y = 0.2.

Table 3 Average Rh particle size (nm) in the catalysts estimated from XRD and TEM

Catalysts	XRD [a]	TEM [b]
RCF(0.0, 0.0)/SiO_2	4.4	4.3
RCF(0.0, 0.2)/SiO_2	4.4	4.2
RCF(0.4, 0.0)/SiO_2	–	2.3
RCF(0.4, 0.2)/SiO_2	–	2.5

[a] Calculated by using the Scherrer equation. [b] Estimated from TEM micrographs by counting more than 150 particles.

Fig. 1 shows the XRD patterns of the reduced catalysts. Two diffraction peaks at 41° and 47° were observed over non-promoted Rh/SiO_2, which are attributed to Rh crystal[39]. Also, a broad diffraction peak attributed to amorphous SiO_2 (2θ = 22°) was observed. The addition of Fe to Rh/SiO_2 did not cause any significant changes compared with non-promoted Rh/SiO_2. However, as the Cr was added to the Rh/SiO_2, the intensity of the diffraction peaks attributed to Rh crystal decreased significantly, indicating that the addition of Cr increased the dispersion of Rh. Fig. 2 shows the TEM images of reduced Rh-Cr-Fe/SiO_2 catalysts with different compositions. The Rh particles were well dispersed over the SiO_2 support in all cases. The sizes of Rh particles calculated from XRD and TEM are listed in Table 2. It can be seen clearly that the size of Rh particles decreased from approximately 4.3 nm to 2.4 nm by addition of Cr to Rh/SiO_2. Some promoters such as Sm[26], Zr[27] and La[37] could also increase the dispersion of Rh particle on silica. Nonetheless, little change in Rh particle size was observed after addition of Fe to Rh/SiO_2. This might be attributed to the fact that the mode of contact between Rh and Cr is different to that between Rh and Fe, which is discussed in more details in section 3.5.

View Article Online
DOI: 10.1039/C5RA28075C

3.4 TPR

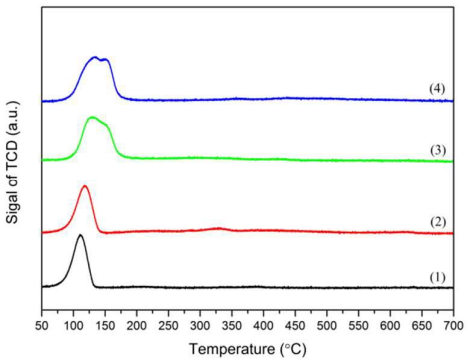

Fig. 3 TPR profiles of RCF(x, y)/SiO_2 catalysts: (1) x = 0.0, y = 0.0; (2) x = 0.0, y = 0.2; (3) x = 0.4, y = 0.0; and (4) x = 0.4, y = 0.2.

The TPR profiles of RCF(x, y)/SiO_2 catalysts are shown in Fig. 3. A single peak at 110 °C was observed in Rh/SiO_2 which is due to the reduction of Rh^{3+}. This peak shifted to 118 °C after the addition of Fe to Rh/SiO_2, indicating the close contact between Rh and Fe, which is in agreement with previous reports in literature[37]. In addition, a weak peak between 300 °C and 350 °C caused by the reduction of Fe^{3+} was also observed over RCF(0.0, 0.2)/SiO_2. In the case of RCF(0.4, 0.0)/SiO_2, a broad peak with a shoulder at around 153 °C was observed. The peak at 128 °C was assigned to the reduction of Rh^{3+}, while the shoulder peak can be attributed to the reduction of Cr species. The results indicated that the addition of Cr or Fe to Rh/SiO_2 inhibited the reduction of Rh^{3+}. Similar phenomenon was also observed over V^{26} or La^{37} promoted Rh/SiO_2 catalysts. On the other hand, simultaneous introduction of Cr and Fe shifted the broad peak to higher temperature with higher peak area, indicating that the reduction of Rh species over RCF(0.4, 0.2)/SiO_2 catalyst was further suppressed and more promoter species got reduced. These results showed that Rh is in intimate contact with Cr and Fe, which might contribute to the improved CO conversion and the selectivity towards ethanol.

3.5 TPSR and FTIR study

As the hydrogenation of carbon to methane is very fast on the Rh-based catalyst, CH_4 formation from chemisorbed CO in H_2 gas flow can provide useful information about the ability of Rh to dissociate CO molecules.[40] Fig. 4 displays the TPSR profiles of the samples. A large CH_4 desorption peak at 100~300 °C and a very small one at 450~550 °C were observed for all the samples studied, which is in lined with the results reported by Liu et al.[2]. The low temperature desorption peak might be attributed to fast hydrogenation of carbon species derived from CO dissociation while the high temperature desorption peak might be due to the hydrogenation of less active carbon species formed at lower temperatures.[2,40] As shown in Fig. 4, Cr and Fe had different effects on the temperature of low temperature desorption peak. In other words, Cr decreased the temperature of the low temperature peak while Fe shifted it to high temperature compared with non-promoted Rh/SiO_2. Therefore, the ability of Rh to dissociate CO molecules was enhanced by the addition of Cr, while it was decreased by the addition of Fe. For Cr- and Fe- promoted Rh/SiO_2, the low temperature desorption peak was located between RCF(0.4, 0.0)/SiO_2 and RCF(0.0, 0.2)/SiO_2, indicating a moderate ability to dissociate CO molecules.

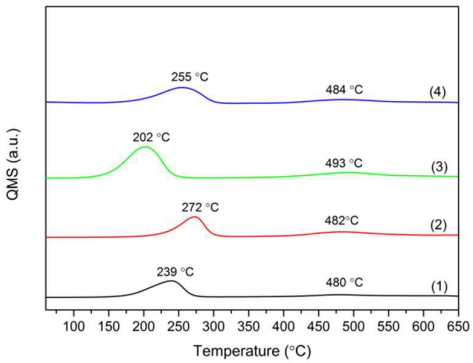

Fig. 4 CH_4 desorption from TPSR of RCF(x, y)/SiO_2 catalysts: (1) x = 0.0, y = 0.0; (2) x = 0.0, y = 0.2; (3) x = 0.4, y = 0.0; and (4) x = 0.4, y = 0.2.

FTIR spectroscopy of adsorbed CO provides an efficient tool to study the interaction between CO and catalysts, which could help determine the surface site that CO resides on.[41] Fig. 5 shows the FTIR spectra of CO adsorbed on RCF(x, y)/SiO_2 catalysts. For non-promoted Rh/SiO_2, two broad peaks at ca. 2042 cm^{-1} and 1897 cm^{-1} were clearly observed, which were attributed to linear CO [CO(l)] and bridged CO [CO(b)] formed on Rh^0 sites, respectively.[41,42] Moreover, two weak peaks at ca. 2092 cm^{-1} and 2026 cm^{-1} also appeared in the CO-FTIR of Rh/SiO_2, which was associated with germinal CO [CO(gdc)] formed on the Rh^+ sites.[41,42] After the addition of Cr to Rh/SiO_2, CO adsorption was enhanced and the position of CO(l) shifted to higher wavenumber slightly. These results indicated that introduction of Cr improved the dispersion of Rh particles[43], which is in line with the results of XRD and TEM. However, after the addition of Fe to Rh/SiO_2, the formation of CO(b) was suppressed. It is well known that CO(b) forms on large Rh particles.[41] Nevertheless, the introduction of Fe to Rh/SiO_2 had negligible effect on the size of Rh particles (Table 3). Thus, FeO_x might tend to cover Rh particle, which does not change the size of Rh particles but decreases the CO(b). On the other hand, introduction of Cr increased the dispersion of Rh particle and the CO adsorption. Therefore, CrO_x likely has a tendency to form in the interface between Rh particles and the support. The proposed contact mode between Rh and the promoters over RCF(x, y)/SiO_2 catalysts was shown in Scheme 1.

The ratio of CO(gdc) versus CO(l) is dependent on the composition of catalysts and these values are listed in Table 2. The ratio was increased to 2.09 and 1.23 for RCF(0.4, 0.0)/SiO_2 and RCF(0.0, 0.2)/SiO_2, respectively, compared with non-promoted Rh/SiO_2. After simultaneous introduction of Cr and Fe to Rh/SiO_2, the ratio of CO(gdc) to CO(l) increased significantly. Therefore, the ratio of Rh^+ sites to Rh^0 sites was

View Article Online
DOI: 10.1039/C5RA28075C

higher over RCF(0.4, 0.2)/SiO_2 compared with RCF(0.4, 0.0)/SiO_2 and RCF(0.0, 0.2)/SiO_2.[44] A growing consensus regarding CO hydrogenation over Rh-based catalysts is that CO dissociates at Rh^0 sites, and that Rh^+ sites are responsible for CO insertion to form intermediates of C_2 oxygenates.[41,44,45] This likely explains why the efficiency of CO insertion over RCF(0.4, 0.2)/SiO_2 was enhanced significantly. It is widely accepted that the main steps for the synthesis of C_2 oxygenates from CO hydrogenation over Rh-based catalysts are: CO dissociation and hydrogenation to form CH_x species, and then CO insertion to form CH_xCO species, followed by hydrogenation, although the exact mechanism is under debate.[46,47] Thus, a good balance between the levels of CO dissociation and insertion is important for efficient synthesis of C_2 oxygenates from CO hydrogenation. Furthermore, addition of Fe to Rh/SiO_2 has been reported to improve the efficiency of the hydrogenation process.[48,49] Thus, high activity and selectivity towards ethanol were obtained over RCF(0.4, 0.2)/SiO_2 with moderate levels of CO dissociation and a high degree of CO insertion.

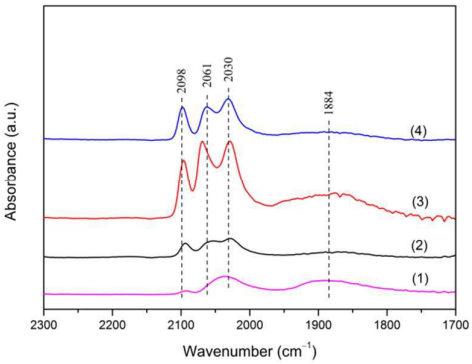

Fig. 5 Infrared spectra of chemisorbed CO on RCF(x, y)/SiO_2 catalysts: (1) x = 0, y = 0.0; (2) x = 0.0, y = 0.2; (3) x = 0.4, y = 0.0; and (4) x = 0.4, y = 0.2.

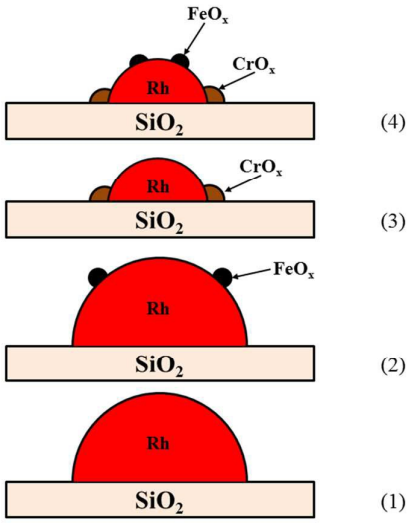

Scheme 1 The proposed contact mode between Rh and promoters over RCF(x, y)/SiO_2 catalysts: (1) x = 0.0, y = 0.0; (2) x = 0.0, y = 0.2; (3) x = 0.4, y = 0.0; and (4) x = 0.4, y = 0.2.

Table 4 Ratios of peak areas for the adsorbed CO species

Catalysts	CO(gdc)/CO(l) [a]
RCF(0.0, 0.0)/SiO_2	0.089
RCF(0.0, 0.2)/SiO_2	1.23
RCF(0.4, 0.0)/SiO_2	2.09
RCF(0.4, 0.2)/SiO_2	3.28

[a] Peak area ratio of CO(gdc) to CO(l) in Fig. 4. Experimental error: ±5%.

4. Conclusions

A series of Cr-promoted and (or) Fe-promoted Rh/SiO_2 catalysts were prepared and investigated in the synthesis of ethanol from CO hydrogenation. TPR showed that Rh was in close contact with Cr and Fe during the catalytic reaction. Furthermore, Cr species showed a tendency to form in the interface between Rh particles and the silica support, while Fe was inclined towards covering the Rh particles, as indicated by the results of XRD, TEM, and FTIR. Addition of Cr to Rh/SiO_2 increased the dispersion of Rh particle and the ability of Rh particles to dissociate CO molecules, while addition of Fe to Rh/SiO_2 increased the degree of CO insertion. A high CO conversion of 10.2% and ethanol selectivity of 26.0% could be obtained over RCF(0.4, 0.2)/SiO_2 with moderate levels of CO dissociation and high efficiency of CO insertion.

References

1 V. Subramani, S. K. Gangwal, *Energy Fuels*, 2008, **28**, 814.
2 W. G. Liu, S. Wang, T. J. Sun, S. D. Wang, *Catal. Lett.*, 2015, **145**, 1741.
3 F. Xue, Y. J. Ding, W. M. Chen, X. G. Song, X. B. Cheng, *React. Kinet. Mech. Catal.*, 2015, **115**, 625.
4 Y. L. Huang, W. H. Deng, E. Guo, P. W. Chung, S. N. Chen, B. G. Trewyn, R. C. Brown, V. S. Y. Lin, *ChemCatChem*, 2012, **4**, 674.
5 X. G. Song, Y. J. Ding, W. M. Chen, W. D. Dong, Y. P. Pei, J. Zang, L. Yan, Y. Lu, *Catal. Commun.*, 2012, **19**, 100.
6 N. D. Subramanian, J. Gao, X. Mo, J. G. Goodwin, W. Torres, J. J. Spivey, *J. Catal.*, 2010, **272**, 204.
7 W. M. Chen, Y. J. Ding, X. G. Song, T. Wang, H. Y. Luo, *Appl. Catal., A*, 2011, **407**, 231.
8 S. R. Wang, W. W. Guo, H. X. Wang, L. J. Zhu, K. Z. Qiu, *Catal. Lett.*, 2014, **144**, 1305.
9 J. G. Nunan, C. E. Bogdan, K. Klier, K. J. Smith, C. W. Young, R. G. Herman, *J. Catal.*, 1988, **113**, 410.
10 J. M. Beiramar, A. G. Constant, A. Y. Khodakov, *ChemCatChem*, 2014, **6**, 1788.
11 T. Matsuzaki, K. Takeuchi, T. A. Hanaoka, H. Arawaka, Y. Sugi, *Appl. Catal., A*, 1993, **105**, 159.
12 J. M. Christensen, A. J. Medford, F. Studt, A. D. Jensen, *Catal. Lett.*, 2014, **144**, 777.

View Article Online
DOI: 10.1039/C5RA28075C

13 A. Cao, G. L. Liu, Y. Z. Yue, L. H. Zhang, Y. Liu, *RSC Adv.*, 2015, **5**, 58804.
14 X. Y. Han, K. G. Fang, Y. H. Sun, *RSC Adv.*, 2015, **5**, 51868.
15 A. Juan, D. E. Damiani, *J. Catal.*, 1992, **137**, 77.
16 Y. Y. Liu, K. Murata, M. Inaba, *React. Kinet. Mech. Catal.*, 2014, **113**, 187.
17 T. Hanaoka, H. Arakawa, T. Matsuzaki, Y. Sugi, K. Kanno, Y. Abe, *Catal. Today*, 2000, **58**, 271.
18 Z. L. Fan, W. Chen, X. L. Pan, X. H. Bao, *Catal. Today*, 2009, **147**, 86.
19 G. van der Lee, B. Schuller, H. Post, T. L. F. Favre, V. Ponec, *J. Catal.*, 1986, **98**, 522.
20 J. Gao, X. H. Mo, A. C. Chien, W. Torres, J. G. Goodwin, *J. Catal.*, 2009, **262**, 119.
21 C. M. Li, J. M. Liu, W. Gao, Y. F. Zhao, M. Wei, *Catal. Lett.*, 2013, **143**, 1247.
22 P. Basu, D. Panayotov, J. T. Yates, *J. Am. Chem. Soc.*, 1998, **110**, 2074.
23 F. Solymosi, I. Tombacz, M. Kocsis, *J. Catal.*, 1982, **75**, 78.
24 D. H. Jiang, Y. J. Ding, Z. D. Pan, W. M. Chen, H. Y. Luo, *Catal. Lett.*, 2009, **121**, 241.
25 J. J. Liu, Z. Guo, D. Childers, N. Schweitzer, C. L. Marshall, R. F. Klie, J. T. Miller, R. J. Meyer, *J. Catal.*, 2014, **313**, 149.
26 H. Y. Luo, W. Zhang, H. W. Zhou, S. Y. Huang, P. Z. Lin, Y. J. Ding, L. W. Lin, *Appl. Catal., A*, 2001, **214**, 161.
27 L. P. Han, D. S. Mao, J. Yu, Q. S. Guo, G. Z. Lu, *Appl. Catal., A*, 2013, **454**, 81.
28 B. M. Weckhuysen, R. A. Schoonheydt, *Catal. Today*, 1999, **51**, 223.
29 H. H. Shin, S. McIntosh, *ACS Catal.*, 2015, **5**, 95.
30 P. Mierczynski, T. P. Maniecki, W. Maniukiewicz, W. K. Jozwiak, *React. Kinet. Mech. Catal.*, 2011, **104**, 139.
31 T. P. Maniecki, P. Mierczynski, W. Maniukiewicz, K. Bawolak, D. Gebauer, W. K. Jozwiak, *Catal. Lett.*, 2009, **130**, 481.
32 M. C. J. Bradford, M. V. Konduru, D. X. Fuentes, *Fuel Process. Technol.*, 2003, **83**, 11.
33 M. Ichikawa, K. Shikakura, M. Kawai, Heterogeneous Catalysis Related to Energy Problems, Proceedings of Symposium, Dalian, China, 1982.
34 V. Schünemann, H. Treviño, G. D. Lei, D. C. Tomczak, W. M. H. Sachtler, K. Fogash, J. A. Dumesic, *J. Catal.*, 1995, **153**, 144.
35 R. Burch, M. J. Hayes, *J. Catal.*, 1997, **165,** 249.
36 R. M. Palomino, J. W. Magee, J. Llorca, S. D. Senanayake, M. G. White, *J. Catal.*, 2015, **329**, 87.
37 X. H. Mo, J. Gao, N. Umnajkaseam, J. G. Goodwin, *J. Catal.*, 2009, **267**, 167.
38 J. Yu, D. S. Mao, L. P. Han, Q. S. Guo, G. Z. Lu, *J. Ind. Eng. Chem.*, 2013, **19**, 806.
39 A. J. Bruss, M. A. Gelesky, G. Machado, J. Dupont, *J. Mol. Catal., A*, 2006, **252**, 212.
40 Y. Wang, H. Y. Luo, D. B. Liang, X. H. Bao, *J. Catal.*, 2000, **196**, 46.
41 S. S. C. Chuang, R. W. Stevens, R. Khatri, *Top. Catal.*, 2005, **32**, 225.
42 M. A. Haider, M. R. Gogate, R. J. Davis, *J. Catal.*, 2009, **261**, 9.
43 T. Beutel, O. S. Alekseev, Y. A. Ryndin, V. A. Likholobov, H. Knözinger, *J. Catal.*, 1997, **169**, 132.
44 J. Yu, D. S. Mao, L. P. Han, Q. S. Guo, G. Z. Lu, *J. Mol. Catal., A*, 2013, **367**, 38.
45 H. Ngo, Y. Y. Liu, K. Murata, *React. Kinet. Mech. Catal.*, 2011, **102**, 425.
46 D. H. Mei, R. Rousseau, S. M. Kathmann, V. A. Glezakou, M. H. Engelhard, W. L. Jiang, C. M. Wang, M. A. Gerber, J. F. White, D. J. Stevens, *J. Catal.*, 2010, **271**, 325.
47 Y. Y. Liu, K. Murata, M. Inaba, I. Takahara, K. Okabe, *Catal. Today*, 2011, **164**, 308.
48 M. M. Bhasin, W. J. Bartley, P. C. Ellgen, T. P. Wilson, *J. Catal.*, 1978, **54**, 120.
49 J. Gao, X. H. Mo, J. G. Goodwin, *J. Catal.*, 2009, **268**, 142.

View Article Online
DOI: 10.1039/C5RA28075C

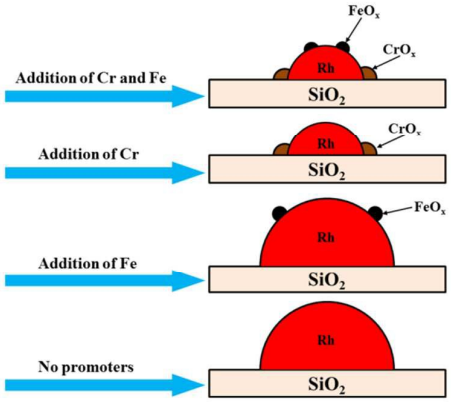

The mode of contact between Rh and Cr is different to that between Rh and Fe.